Supporting Information

N,S Co-doped 3D Mesoporous Carbon-$Co_3Si_2O_5(OH)_4$ Architectures for High-Performance Flexible Pseudo-Solid-State Supercapacitor

*Xinran Li[a], Shiyuan Ding[a], Xiao Xiao[a] , Jinying Shao[a], Jilei Wei[a], Huan Pang[a]*and Yan Yu[b]**

a. *College of Chemistry and Chemical Engineering, Yangzhou University Yangzhou, Jiangsu, 225002, Jiangsu, P. R. China, E-mail: huanpangchem@hotmail.com; panghuan@yzu.edu.cn.*

b. *CAS Key Laboratory of Materials for Energy Conversion, Department of Materials Science and Engineering, University of Science and Technology of China, Hefei 230026, Hefei, P. R. China. E-mail: yanyumse@ustc.edu.cn*

Calculations

The mass-specific capacitance ($C/F\ g^{-1}$) of the device can also be calculated using：

$$C=Q / (m\times\Delta V)=\int Idt / (m\times\Delta V)= I\times t_{discharge} / (m\times\Delta V) \quad (1)$$

Where m is the mass of the activated materials, I is the discharge current, $t_{discharge}$ is discharge time, and ΔV is the potential drop during discharge.

The area-specific capacitance ($C/mF\ cm^{-2}$) of the device can also be calculated using：

$$C=Q / (A\times\Delta V)=\int Idt / (A\times\Delta V)= I\times t_{discharge} / (A\times\Delta V) \quad (2)$$

Where A is the surface area of the device, I is the discharge current, $t_{discharge}$ is discharge time, and ΔV is the potential drop during discharge.

The energy density and power density of the device can be obtained from：

$$E=0.5C\times V^2 \quad (3)$$

$$P=E/t_{discharge} \quad (4)$$

Where V represents the operating voltage.

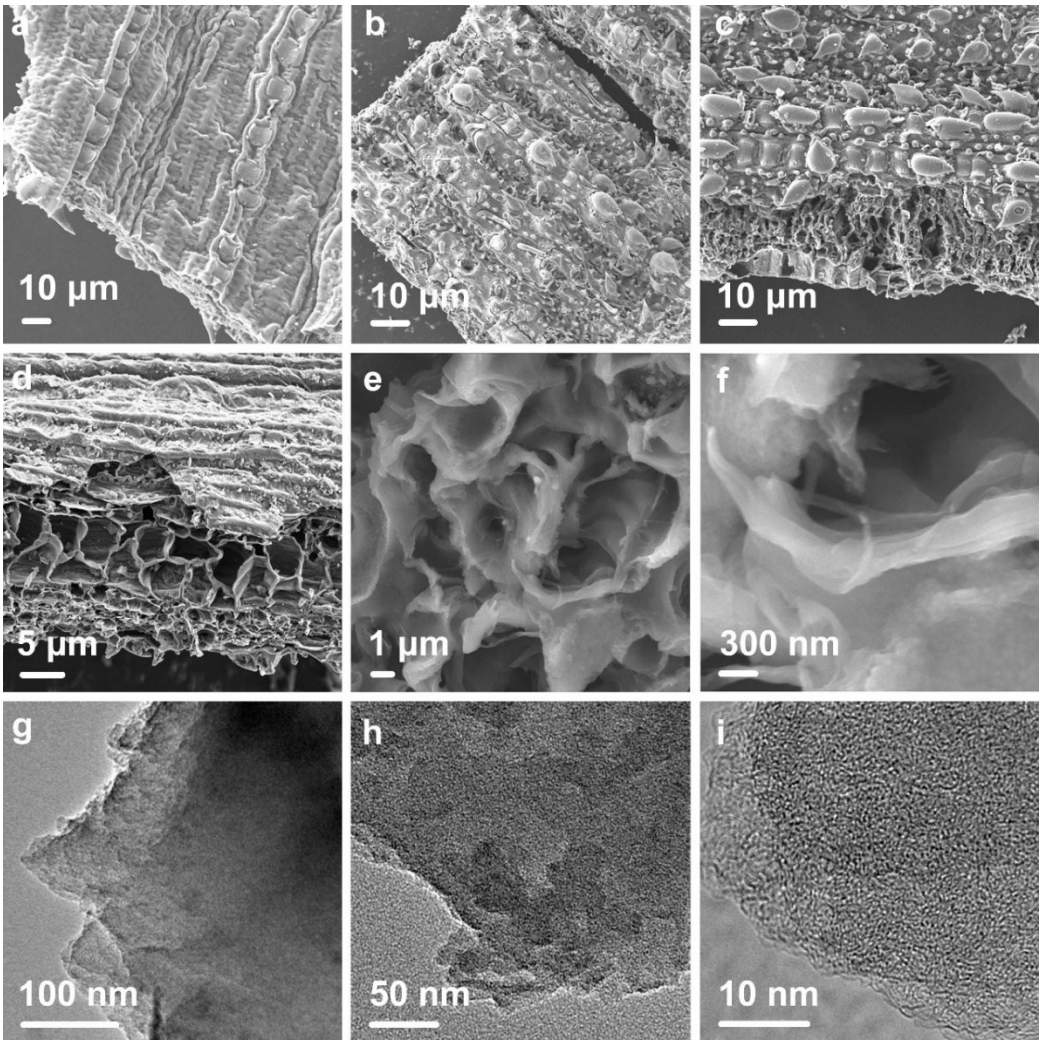

Figure S1. a-f) SEM images of as-prepared samples (N,S co-doped 3D mesoporous C-SiO_2 architectures), and g-i) Corresponding TEM images.

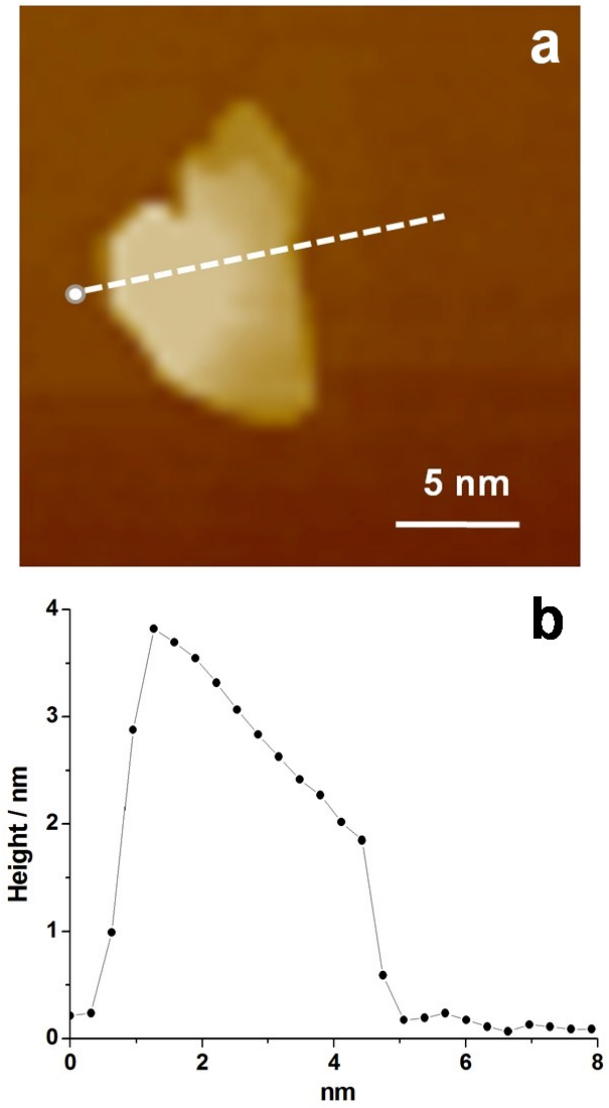

Figure S2. Atomic force microscope (AFM) image of $Co_3Si_2O_5(OH)_4$ ultrathin nanoflakes.

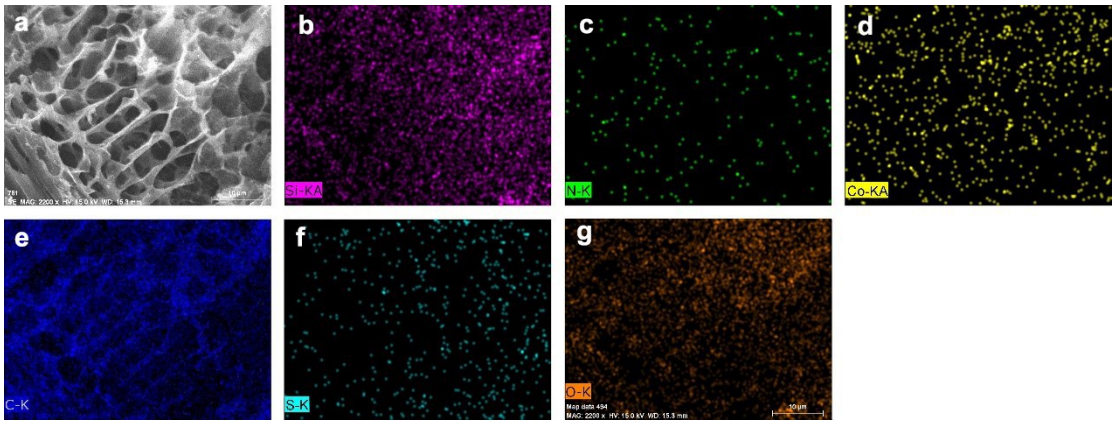

Figure S3. The corresponding EDS mappings of N,S co-doped 3D mesoporous C-$Co_3Si_2O_5(OH)_4$ architectures: a) SEM image, b) Purple-Si-K, c) Green-N-K, d) Yellow-Co-K, e) Blue-C-K, f) Cyan-S-K, and g) Orange-O-K, respectively.

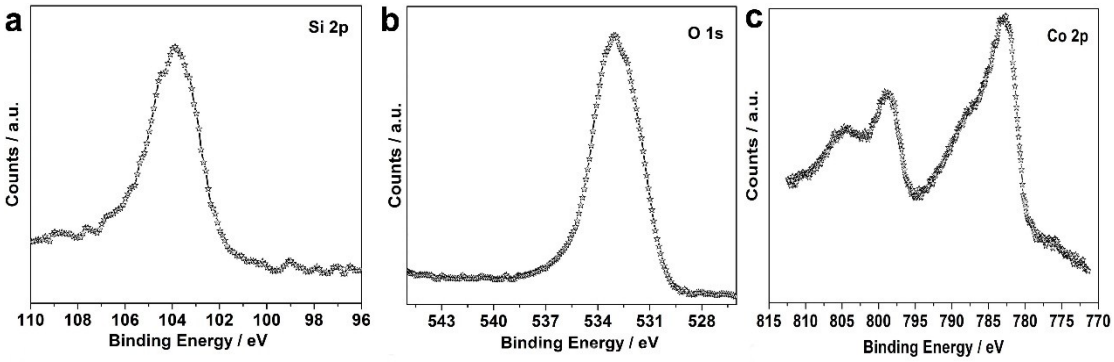

Figure S4. The high-resolution spectra of the N,S co-doped 3D mesoporous C-$Co_3Si_2O_5(OH)_4$ architectures (a) Si 2p, (b) O 1s, and (c) Co 2p.

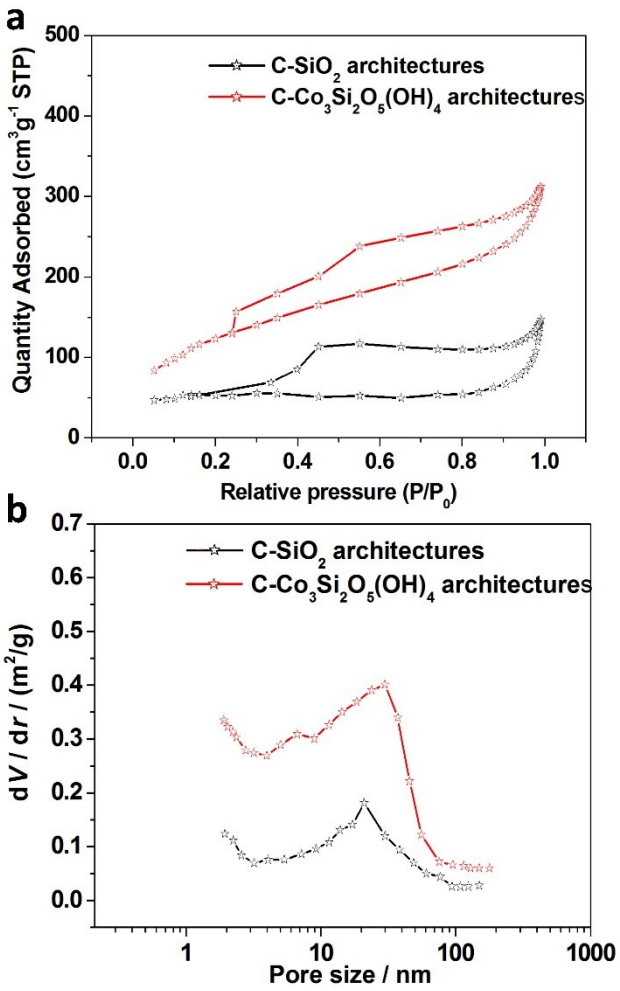

Figure S5. a) N_2 adsorption-desorption isotherm, and (b) the corresponding pore size distribution curve of as-prepared samples (3D mesoporous C-SiO_2 architectures, and N,S co-doped 3D mesoporous C-$Co_3Si_2O_5(OH)_4$ architectures).

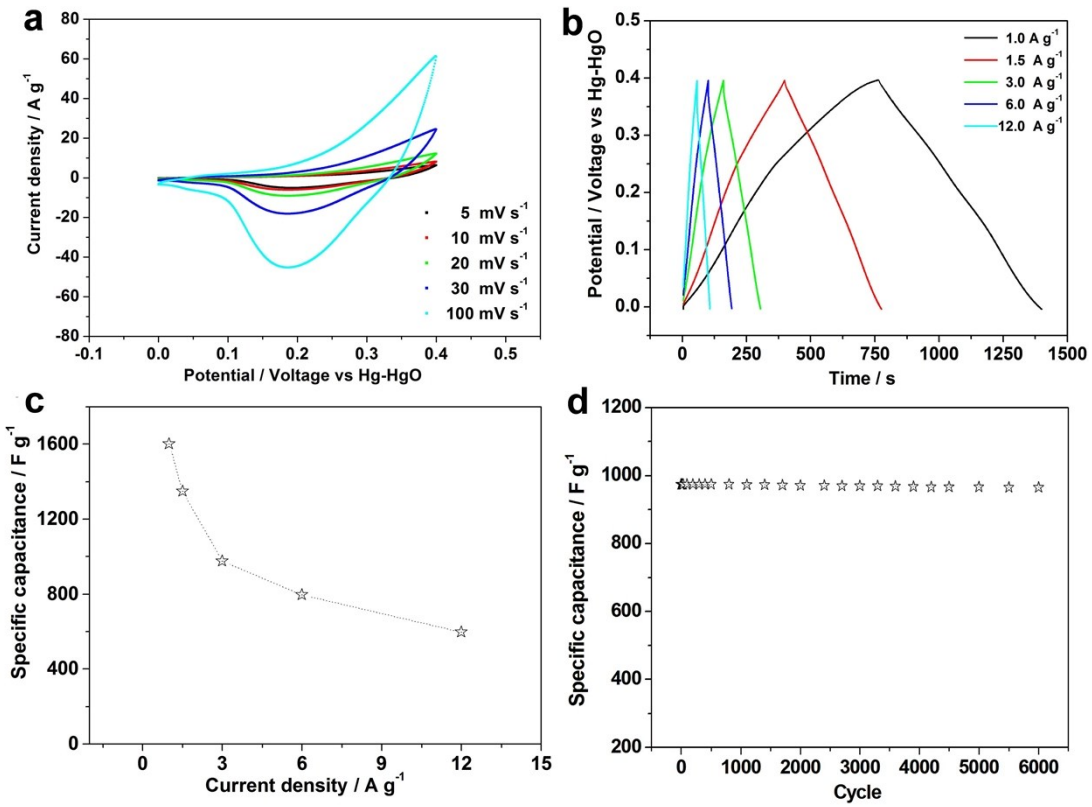

Figure S6. a) Cyclic voltammetry within 0 to 0.4 V range at different scan rates of 5-100 $mV \cdot s^{-1}$ was performed on the as-prepared electrodes in 3.0 M KOH at room temperature, b) The galvanostatic discharge curves at 1.0-12.0 A g^{-1}, c) Specific capacitance obtained from different current densities，and d) Cycling performance of the device at 3.0 A g^{-1} for 6000 cycles.

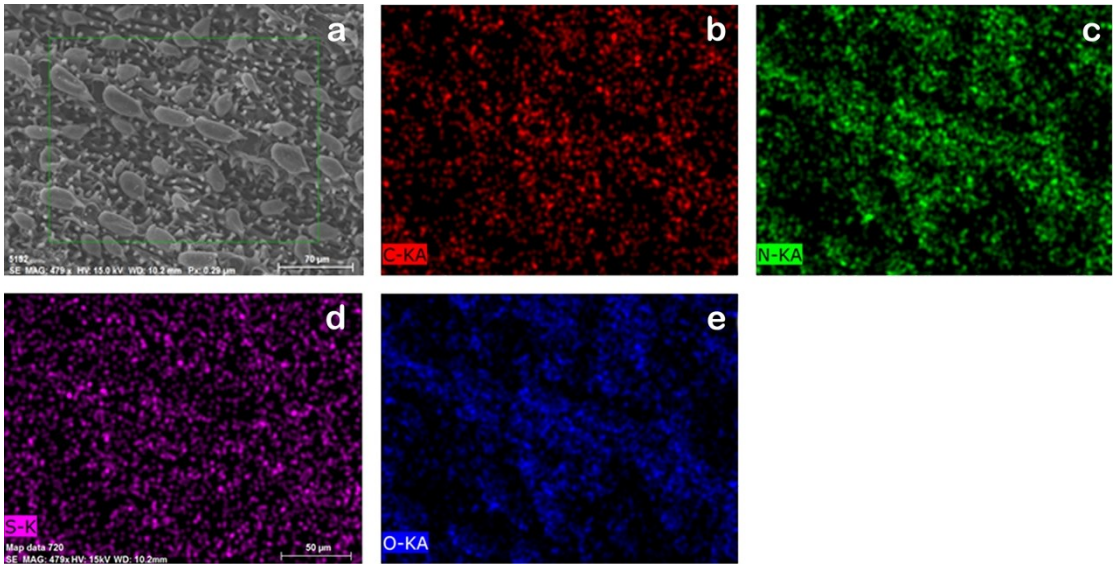

Figure S7. The corresponding EDS mappings of N,S co-doped pure carbon architectures (600 ^{o}C): a) SEM image, b) Red-C-K, c) Green-N-K, d) Purple-S-K, e) Blue-O-K, respectively.

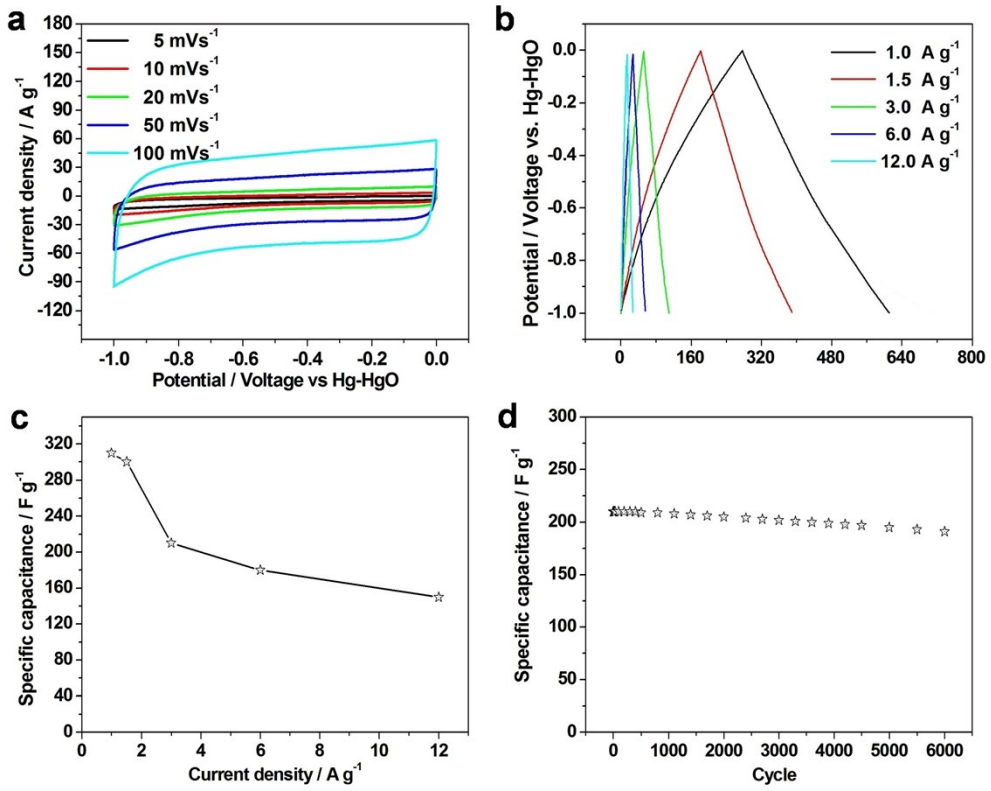

Figure S8. a) Cyclic voltammetry within -1.0 to 0 V range at different scan rates of 5-100 $mV \cdot s^{-1}$ was performed on the as-prepared N,S co-doped pure carbon architectures (600 ^{o}C) electrodes in 3.0 M KOH at room temperature, b) The galvanostatic discharge curves at 1.0-12.0 A g^{-1}, c) Specific capacitance obtained from different current densities, and d) Cycling performance of the device at 3.0 A g^{-1} for 6000 cycles.

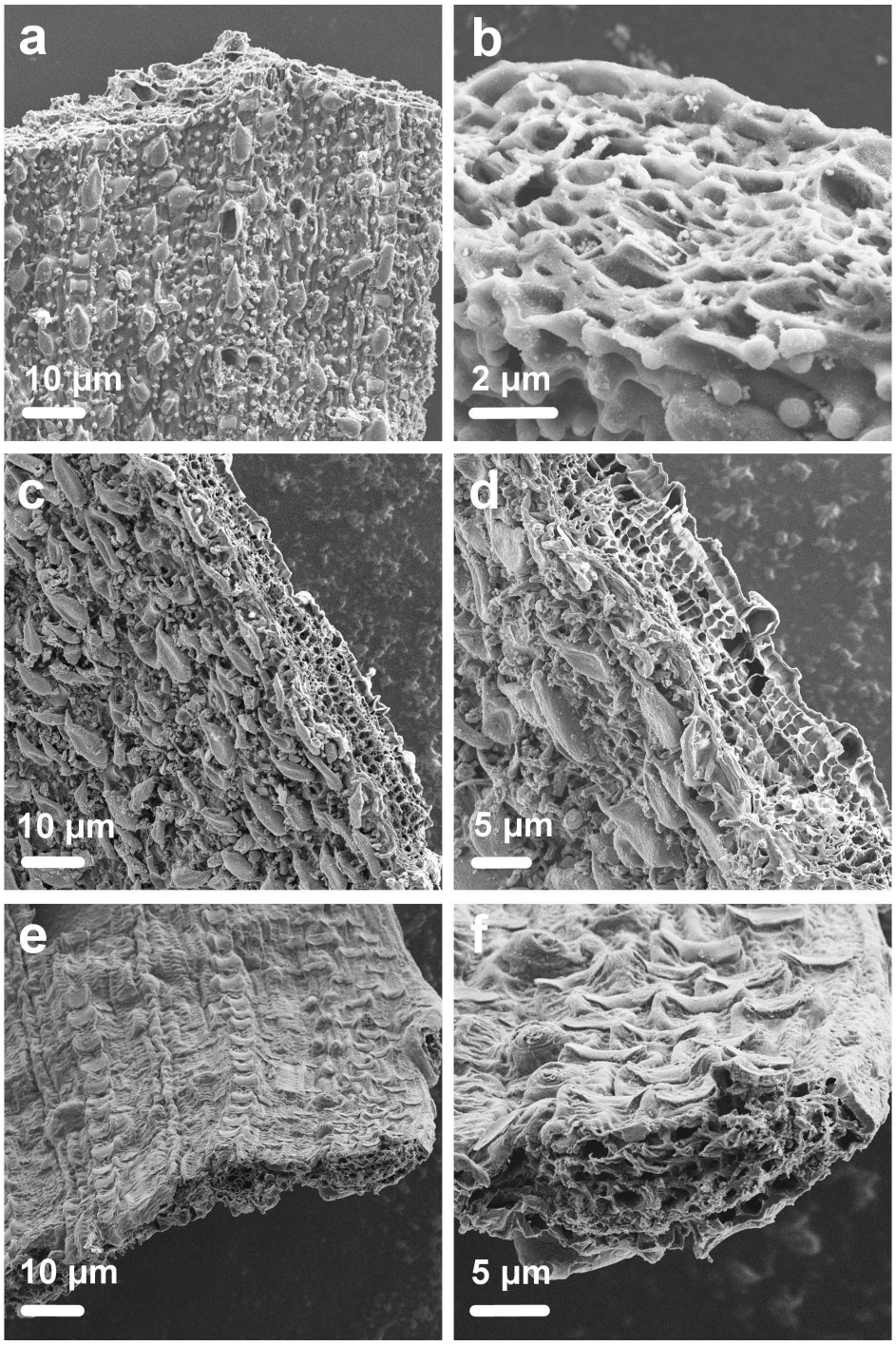

Figure S9 SEM images of N,S co-doped pure carbon architectures obtained with different calcination temperatures: a, b) 600 °C, c, d) 800 °C and e, f) 900 °C.

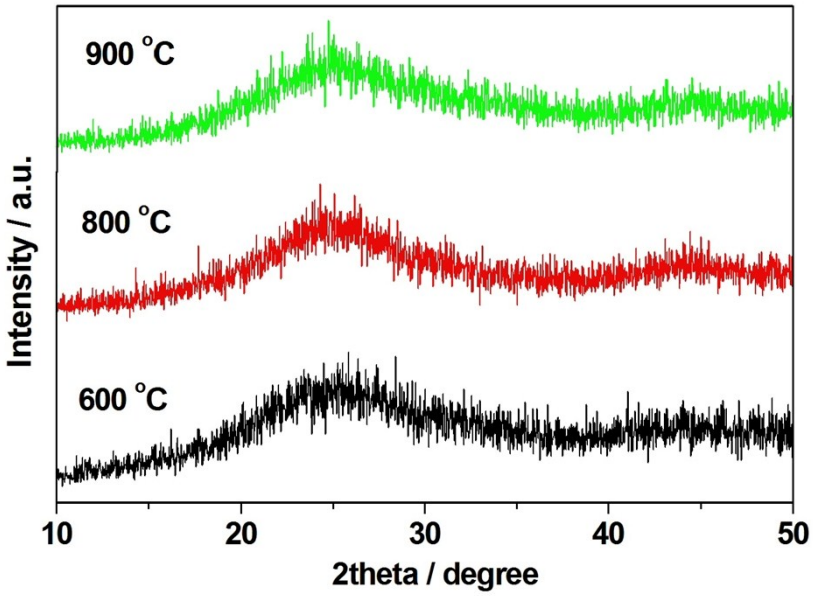

Figure S10 XRD patterns of N,S co-doped pure carbon architectures obtained with different calcination temperatures: 600 °C, 800 °C and 900 °C.

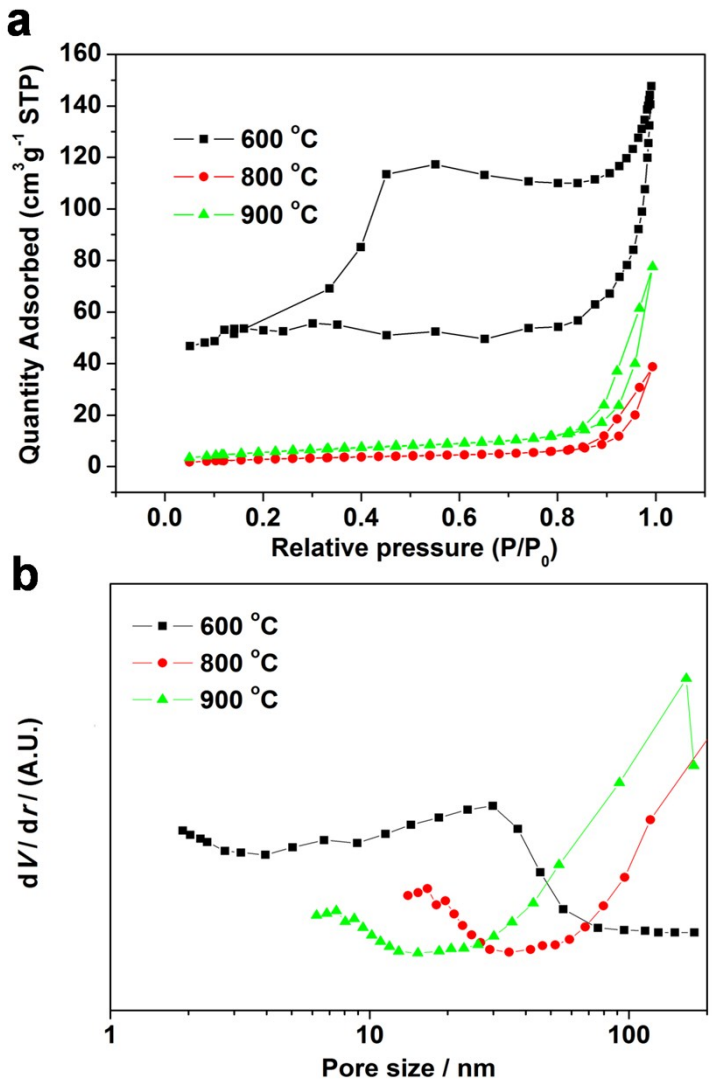

Figure S11. a) The corresponding N_2 adsorption-desorption isotherms, and b) The corresponding pore size distribution curve of N,S co-doped pure carbon architectures obtained with different calcination temperatures: 600 ^{o}C, 800 ^{o}C and 900 ^{o}C.

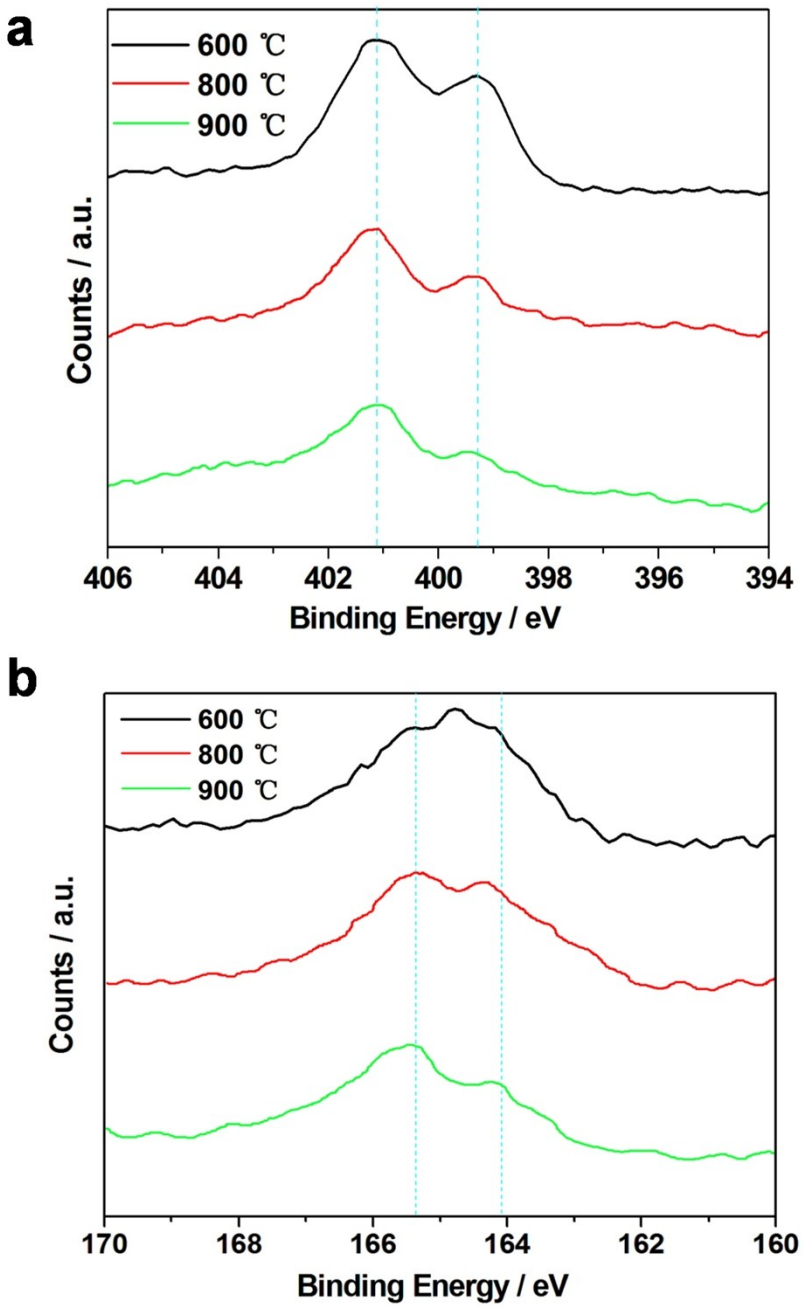

Figure S12. The high-resolution XPS spectra of N,S co-doped pure carbon architectures obtained with different calcination temperatures: 600 ^{o}C, 800 ^{o}C and 900 ^{o}C, a) N 1s, and b) S 2p.

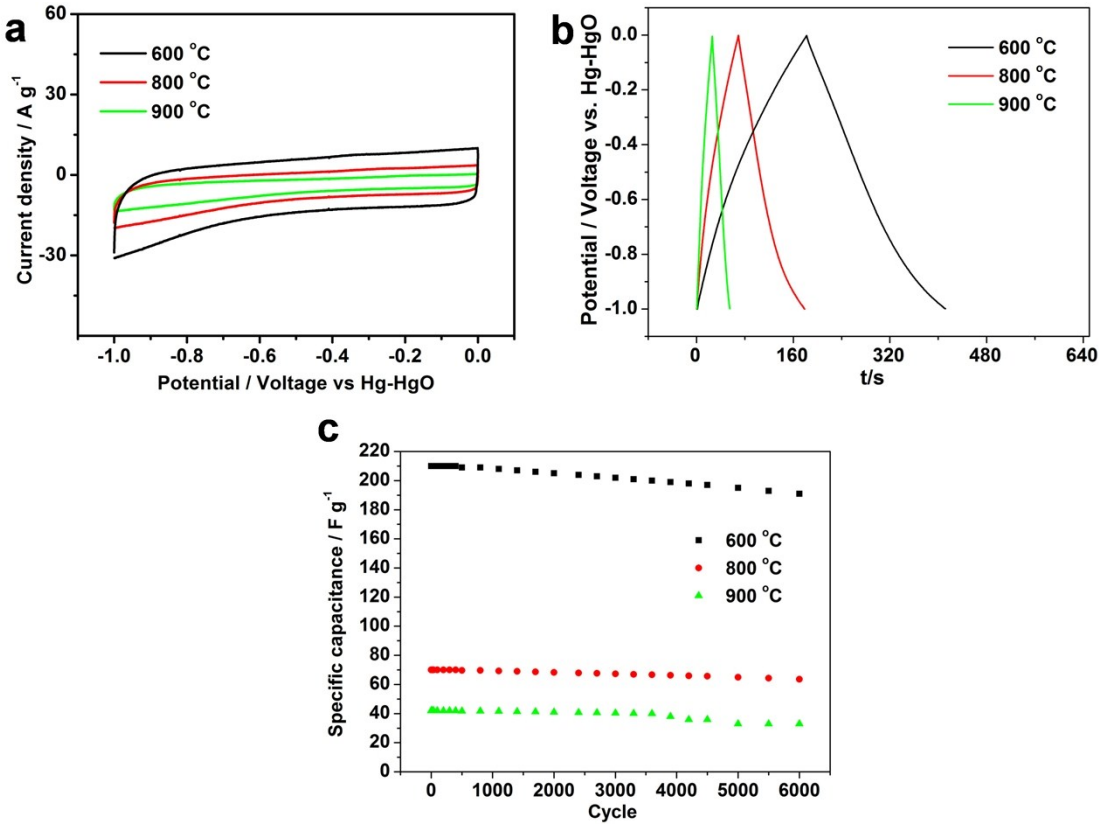

Figure S13. The as-prepared N,S co-doped pure carbon architectures (600 °C, 800 °C and 900 °C) electrodes in 3.0 M KOH at room temperature: a) Cyclic voltammetry within -1.0 to 0 V range at a scan rate of 20 $mV \cdot s^{-1}$, b) The galvanostatic discharge curves at 1.5 A g^{-1}, and c) Cycling performance of the device at 3.0 A g^{-1} for 6000 cycles.

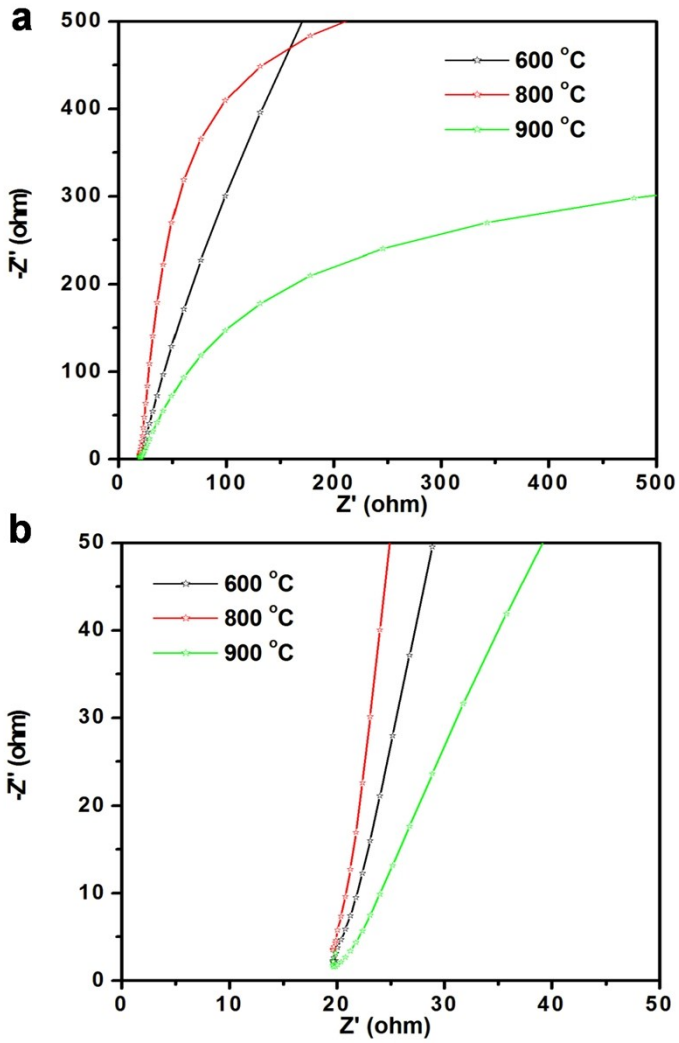

Figure S14. Electrochemical impedance spectra (EIS) image of the the as-prepared N,S co-doped pure carbon architectures (600 °C, 800 °C and 900 °C) electrodes in 3.0 M KOH, a) 0-500 Ohm, and b) 0-50 Ohm.

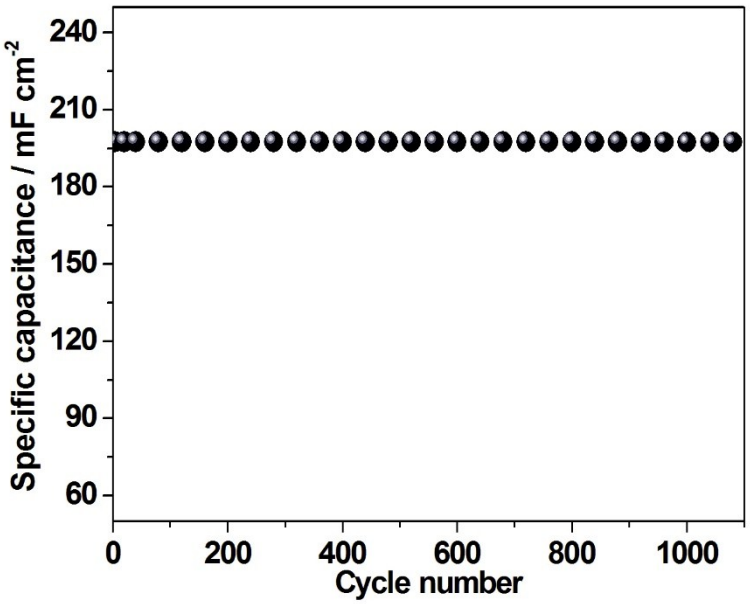

Figure S15. The mechanical stability (1000 cycles of bending 90^{o} at 8.0 Am cm^{-2}) of the NS-C-CoSiO//Activated carbon flexible solid-state asymmetric supercapacitors.

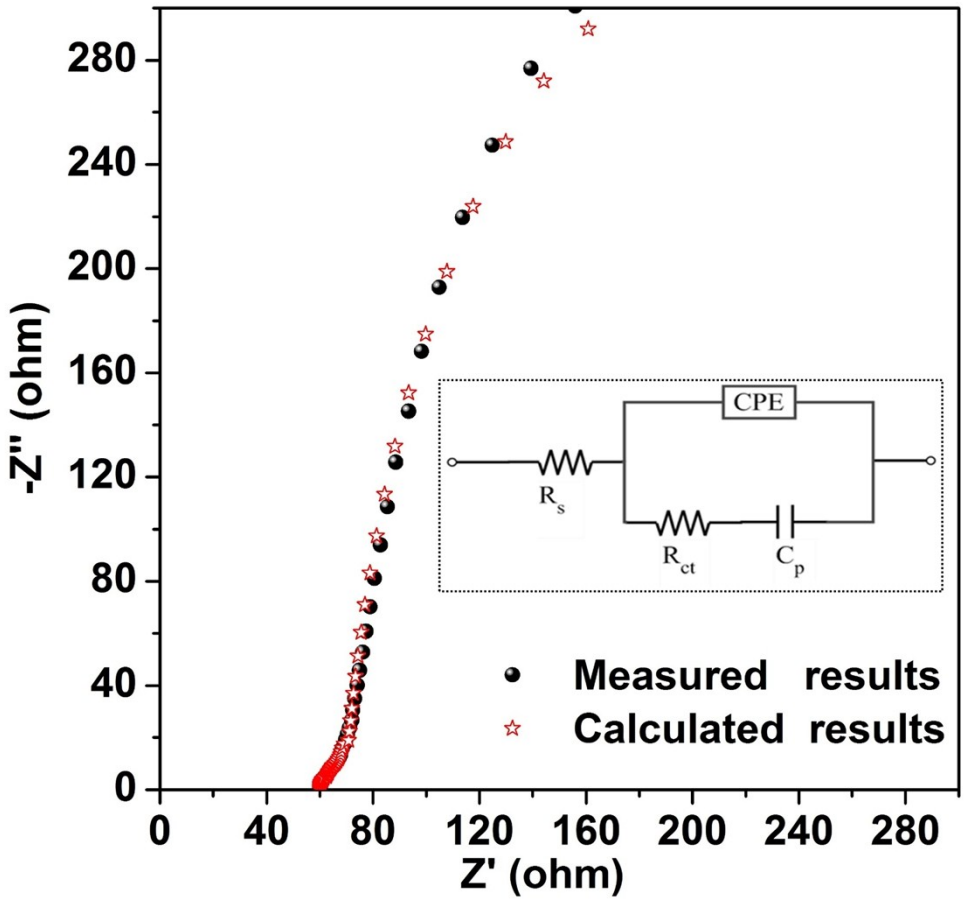

Figure S16. Electrochemical impedance spectra (EIS) image of the NS-C-CoSiO // activated carbons device.

Table S1. The Co/Si weight% is further analyzed and confirmed by inductively coupled plasma-atomic emission spectrometry (ICP-AES), and the atom ratio of Co/Si is 3.01:2.

Element	W/%
Co	22.3
Si	7.1

Table S2. Some previous Co-based nanomaterials for supercapacitor in three-electrode system.[1-21]

Micro/nanostructures	**Capacitance, 1 A g^{-1} / F g^{-1}**	**Ref.**
β-$Co(OH)_2$ single layer	2028	1
Ni,Co-OH/GO sheets	1540	2
Co_3O_4 thin sheets	1500	3
Ni-Co-S nanoparticles	1492	4
The MnO_2-NPs@Co/C	1050	5
$NiCo_2O_4$/GO composites	1211.25	6
$LiCoO_2$ particles	1050	7
$NiCo_2S_4$ ball-in-ball hollow spheres	1036	8
$Ni_xCo_{3-x}O_4$ nanoparticles	800	9
CoFS sheets	711.3	10
Co_3O_4 nanotubes	647	11
$CoCO_3$/CoO/carbon cloth	510	12
Mesoporous Co_3O_4 nanoflakes	450	13
Co_3O_4@CNT/polyindole composite	442.5	14
Co_2P nanoflake/carbon cloth	430	15
$Co_2(OH)_2CO_3$/activated carbon	301.44	16
$Co_{0.85}Se$//N-PCNs	290	17
α-$Co(OH)_2$/carbon nanofoam	210	18
$CoMoO_4$ nanospheres	170	19
Layered $(Ni,Co)_3Si_2O_5(OH)_4$	150	20
Hollow porous Co_3O_4 nanospheres	150	21
3D mesoporous C-$Co_3Si_2O_5(OH)_4$	***1600***	***This work***

Table S3. The N and S content of as-prepared N,S co-doped pure carbon architectures (600 ^{o}C, 800 ^{o}C and 900 ^{o}C).

	N wt %	**S wt %**
Sample-600	2.7	1.8
Sample-800	1.5	0.7
Sample-900	0.8	0.4

Table S4. The N/C and S/C atomic ratio of as-prepared N,S co-doped pure carbon architectures (600 ^{o}C, 800 ^{o}C and 900 ^{o}C).

	N/C(%)	**S/C(%)**
Sample-600	2.4	0.7
Sample-800	1.3	0.3
Sample-900	0.7	0.2

Table S5. The percentages of the graphitic-N, pyridinic-N, and pyrrolic-N of as-prepared N,S co-doped pure carbon architectures (600 ^{o}C, 800 ^{o}C and 900 ^{o}C).

	Pyridinic-N(%)	**Pyrrolic-N(%)**	**Graphitic-N(%)**
Sample-600	35.2	33.8	31
Sample-800	33.9	35.6	30.5
Sample-900	31.6	34.8	33.6

References

[1] S. Gao, Y. F. Sun, F. C. Lei, L. Liang, J. W. Liu, W. T. Bi, B. C. Pan, Y. Xie, *Angew. Chem. Int. Ed.,* 53 (2014) 12789.

[2] H. Ma, J. He, D. B. Xiong, J. S. Wu, Q. Q. Li, V. Dravid, Y. F. Zhao, *ACS Appl. Mater. Inte.,* 8 (2016) 1992.

[3] Y. Q. Jiang, L.Y. Chen, H. Q. Zhang, Q. Zhang, W. F. Chen, J. K. Zhu, D. M. Song, *Chem. Eng. J.,* 292 (2016) 1.

[4] J. Yang, C. Yu, X. M. Fan, S. X. Liang, S. F. Li, H. W. Huang, Z. Ling, C. Hao, J. S. Qiu, *Energy Environ. Sci.,* 9 (2016) 1299.

[5] J. Zhi, O. Reiser, F. Q. Huang, *ACS Appl. Mater. Inte.,* 8 (2016) 8452.

[6] Y. J. Xu, L. C. Wang, P. Q. Cao, C. L. Cai, Y. B. Fu, X. H. Ma, *J. Power Sources,* 306 (2016) 742.

[7] Y. N. Xu, Y. Y. Dong, X. Han, X. F. Wang, Y. J. Wang, L. F. Jiao, H. T. Yuan, *ACS Sustainable Chem. Eng.* 3 (2015) 2435.

[8] L. F. Shen, L. Yu, H. B. Wu, X. Y. Yu, X. G. Zhang, X. W. (David) Lou, *Nat. Commun.,* (2015) DOI:10.1038/ncomms7694.

[9] S. R. Chen, M. Xue, Y. Q. Li, Y. Pan, L. K. Zhu, S. L. Qiu, *J. Mater. Chem. A*, 3 (2015) 20145.

[10] W. Yang, Y. Y. Feng, N. Wang, H. Y. Yuan, D. Xiao, *J. Alloy. Compd.,* 644 (2015) 836.

[11] H. Li, F. Yue, C. Yang, P. Qiu, P. Xue, Q. Xu, J. D Wang, *Ceram. Int.* 42 (2016) 3121.

[12] J. Xu, S. Cheng, L. F. Yang, Y. Jiang, Z. J. Jiang, C. H. Yang, H. Zhang, M. L. Liu, *Nano Energy,* 11 (2015) 736.

[13] A. G. Xiao, S. B. Zhou, C. G. Zuo, Y. B. Zhuan, X. Ding, *Mater. Res. Bull*. 60 (2014) 674.

[14] X. Zhou, A. Q. Wang, Y. M. Pan, C. F. Yu, Y. Zou, Y. Zhou, Q. Chen, S. S. Wu, *J. Mater. Chem. A,* 3 (2015) 13011.

[15] X. J. Chen, M. Cheng, D. Chen, R. M. Wang, *ACS Appl. Mater. Inte.* 8 (2016) 3892.

[16] T. M. Masikhwa, J. K. Dangbegnon, A. Bello, M. J. Madito, D. Momodu, N. Manyala, *J. Phys. Chem. C,* 88 (2016) 60.

[17] H. Peng, G. F. Ma, K. J. Sun, Z. G. Zhang, J. D. Li, X. Z. Zhou, Z. Q. Lei, *J. Power Sources.* 297 (2015) 351.

[18] R. D. Noce, S. Eugenio, T. M. Silva, M. J. Carmezim, M. F. Montemor, *J. Power Sources.* 288 (2015) 234.

[19] M. J. Barmi, M. M. Sundaram, *RSC Adv.* 6 (2016) 36152.

[20] Q. Rong, L. L. Long, X. Zhang, Y. X. Huang, H. Q. Yu, *Appl. Energ.* 153 (2015) 63.

[21] F. L. Meng, Z. G. Fang, Z. X. Li, W. W. Xu, M. J. Wang, Y. P. Liu, J. Zhang, W. R. Wang, D. Y. Zhao, X. H. Guo, *J. Mater. Chem. A*. 1 (2013) 7235.